

# We are IntechOpen, the world's leading publisher of Open Access books Built by scientists, for scientists

6,900

Open access books available

186,000

International authors and editors

200M

Downloads

Our authors are among the

154

Countries delivered to

TOP 1%

most cited scientists

12.2%

Contributors from top 500 universities



WEB OF SCIENCE™

Selection of our books indexed in the Book Citation Index  
in Web of Science™ Core Collection (BKCI)

Interested in publishing with us?  
Contact [book.department@intechopen.com](mailto:book.department@intechopen.com)

Numbers displayed above are based on latest data collected.  
For more information visit [www.intechopen.com](http://www.intechopen.com)



---

# Interferometer Instantaneous Frequency Identifier

---

M. T. de Melo, B. G. M. de Oliveira,  
Ignacio Llamas-Garro and Moises Espinosa-Espinosa

Additional information is available at the end of the chapter

<http://dx.doi.org/10.5772/52623>

---

## 1. Introduction

The rapid development of radar, communication and weapons guidance systems generates an urgent need for microwave receivers to detect possible threats at the earliest stage of a military mission. The microwave receivers used to intercept the RF signals must be able to meet these challenges. Thus, microwave receivers have become an important research area because of their applications to electronic warfare (EW) [1].

The instantaneous frequency measurement (IFM) receiver has been mostly incorporated in advanced EW systems. As to perform the fundamental function, which is to detect threat signals and provide information to the aircrafts, ships, missiles or ground forces, the IFM receiver offers high probability of intercept over wide instantaneous RF bandwidths, high dynamic ranges, moderately good sensitivity, high frequency measurement accuracy, real time frequency measurement and relatively low cost.

IFM started out as a simple technique to extract digital RF carrier frequency over a wide instantaneous bandwidth mainly for pulsed RF inputs. It is been gradually developed to a resourceful system for real time encoding of the RF input frequency, amplitude, pulse width, angle of arrival (AOA) and time of arrival (TOA) for both pulsed and continuous wave (CW) RF inputs. For many electronic support measures (ESM) applications, the carrier frequency is considered to be one of the most important radar parameters, since it is employed in many tasks: sorting, even in dense signal environments; emitter identification and classification; and correlation of similar emitter reports from different stations or over long time intervals, to allow emitter location [2,3].

An IFM receiver is an important component in many signal detection systems. Though numerous improvements have been made to the design of these systems over the years, the basic principle of operation remains relatively unchanged, in that the frequency of an in-

coming signal is converted into a voltage proportional to the frequency. Microwave interferometers are usually base circuits of the IFM systems. These interferometers most often consist of directional couplers, power combiners/dividers and delay lines [4-8]. As a good example, a coplanar interferometer based on interdigital delay line with different finger lengths, will be presented. Another example of interferometers, but now, implemented with micro strip multi-band-stop filters to obtain signals similar to those supplied by the interferometers was published recently and will be presented here as well [9,10].

## 2. Important concepts

The system is based on frequency mapping, going from analogical signal into digital words. Any frequency value in the operating band of the system corresponds to a unique digital word. In the process, there is no need to adjust or tune any device. The signal is identified instantaneously. The frequency resolution depends on the longest delay and the number of discriminators.

Let us see how the IFMS maps the incoming signal  $x(t)$  into digital words. First of all, consider a sinusoidal signal  $x(t) = \sin(\omega t)$  split into two parts, as shown in Fig. 1.

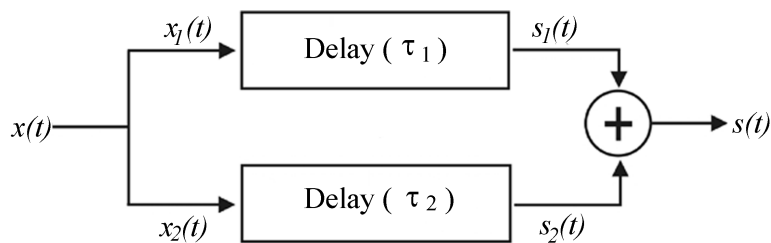


**Figure 1.** Interferometer used in instantaneous frequency measurement subsystem.

The signals  $x_1(t)$  and  $x_2(t)$  are then described as

$$x_1(t) = x_2(t) = \frac{\sin(\omega t)}{2} \tag{1}$$

Because of different delays  $\tau_1$  and  $\tau_2$ , one has

$$s_1(t) = x_1(t - \tau_1) \tag{2}$$

and

$$s_2(t) = x_2(t - \tau_2). \tag{3}$$

$S_1(t)$  and  $S_2(t)$  are the signals after passing the delay  $\tau_1$  and  $\tau_2$ , respectively. Then the output  $s(t)$  is given by the addition of (2) and (3), and after some trigonometric manipulations that sum can be written as

$$s(t) = \sin\left(\frac{2\omega t - \omega(\tau_1 + \tau_2)}{2}\right) \cos\left(\frac{\omega(\tau_2 - \tau_1)}{2}\right). \quad (4)$$

From (4), one can see that the frequency interval between two consecutive maxima or minima of  $s(t)$  are given by

$$\Delta f = \left| \frac{1}{\Delta\tau_{2,1}} \right|, \quad (5)$$

where  $\Delta\tau_{2,1} = \tau_2 - \tau_1$  is the delay difference between the two branches of the interferometer. Still from (5), it is noticed that from  $\Delta f_{\max}$  one gets  $\Delta\tau_{\min}$  and vice-versa.

As in [1], the frequency resolution is given by

$$f_R = \frac{1}{4 \Delta\tau_{\max}}. \quad (6)$$

A binary code can be generated if

$$\Delta\tau_{\max} = 2^{n-1} \Delta\tau_{\min}, \quad (7)$$

And this way, the resolution  $f_r$  of an  $n$ -bits subsystem can be rewritten as

$$f_R = \frac{1}{2^{n+1} \Delta\tau_{\min}}. \quad (8)$$

Fig. 2 shows the architecture of a traditional instantaneous frequency measurement subsystem (IFMS), where delay lines are used to implement five interferometers as discrimination channels.

Each discriminator provides one bit of the output binary word that is assigned to a certain sub-band of frequency [1]. Wilkinson power dividers are used at the input and output of each interferometer [3]. The output of each discriminator is connected to a detector. The 1 bit A/D converter receives the signal from the amplifier, and attributes "0" or "1" to the output to form the digital word for each frequency sub-band. These values depend on the power level of the received signal. A limiting amplifier is used in IFM input to control the signal gain, to increase sensitivity, and clean up the signal within the band of interest [1], [7].

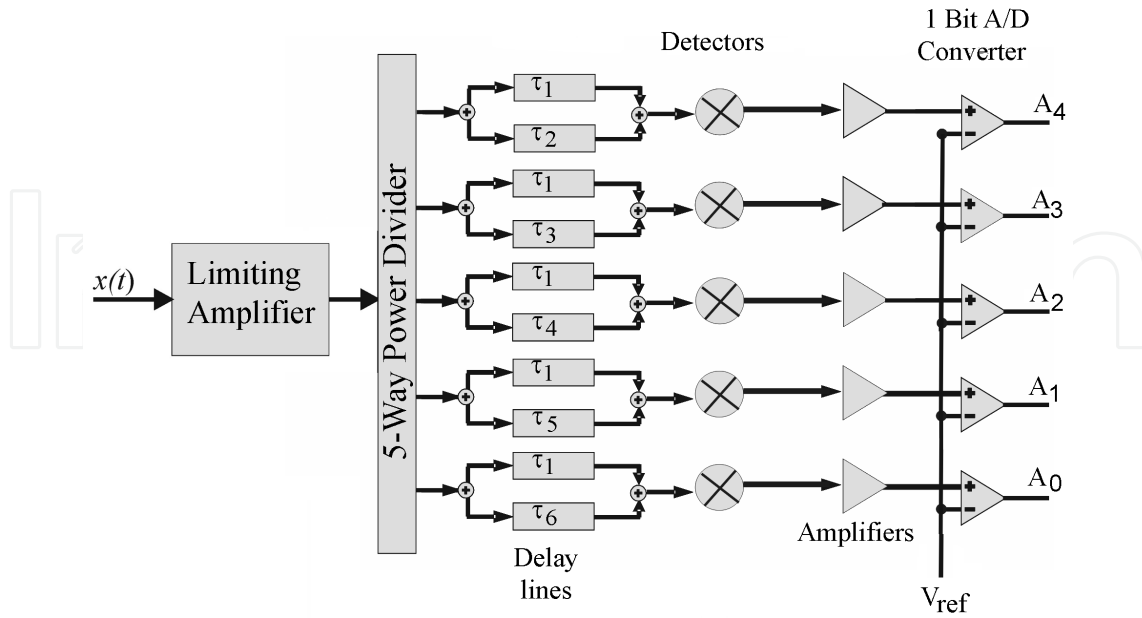


Figure 2. Architecture of a traditional IFM subsystem.

### 3. Coplanar interdigital delay Line for IFM systems

The schematic drawing of the interdigital delay is shown in figure 3. The particular line consists of 164 interdigital fingers of equal length  $\ell$ , finger width  $w$ , finger spacing  $s$  and total length  $L$ .  $d$  is the unit cell length representing the periodicity of the transmission line. If  $d \ll \lambda$ , an amount of lumped capacitance per unit length  $C_0/d$  is added to the shunt capacitance  $C$ .

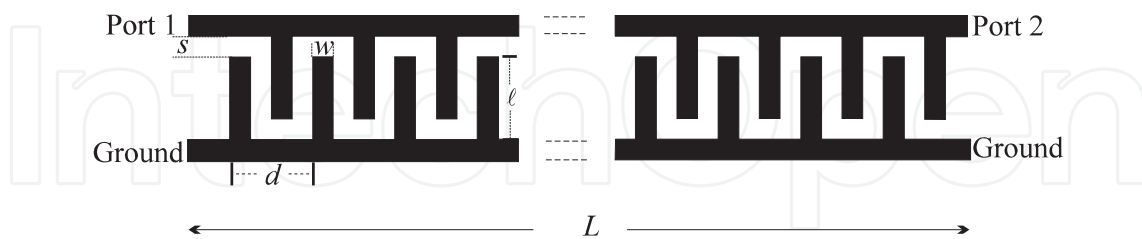


Figure 3. Coplanar interdigital delay line under test.

For the structure shown in figure 3 the phase velocity and the characteristic impedance  $Z_0$ , become:  $[(C + 2C_0/d) L_s]^{-1/2}$  and  $[L_s / (C + 2 C_0/d)]^{1/2}$ , respectively. Here,  $L_s$  is the series inductance [11]. Due to the fringing electric fields about the fingers, the amount by which the capacitance per unit length increases is greater than the corresponding amount by which the inductance per unit length decreases. In order to exploit the fringing electric fields produced by the fingers, one needs to increase the finger length and keep the finger width fixed.

The  $ABCD$  matrix of a lossless transmission line section of length  $L$ , line impedance  $Z_0$  and phase constant  $\beta$  is given by

$$\begin{bmatrix} A & B \\ C & D \end{bmatrix} = \begin{bmatrix} \cos(\beta L) & jZ_0 \sin(\beta L) \\ (1/Z_0)j \sin(\beta L) & \cos(\beta L) \end{bmatrix} \quad (9)$$

From the above equation one can relate  $Z_0$  to only  $B$  and  $C$  elements. If we use the conversion from  $ABCD$  matrix to  $S$ -parameters and assume the source and load reference impedance as  $Z$ , we then have [12]

$$Z_0 = \sqrt{\frac{B}{C}} = \left[ Z^2 \frac{(1+S_{11})(1+S_{22}) - S_{12}S_{21}}{(1-S_{11})(1-S_{22}) - S_{12}S_{21}} \right]^{1/2} \quad (10)$$

Note that the  $ABCD$  matrix is not for a unit cell of the line, it represents the entire transmission line.

Group delay is the measurement of signal transmission time through a test device. It is defined as the derivative of the phase characteristic with respect to frequency. Assuming linear phase change  $\phi_{21}(2)\phi_{21}(1)$  over a specified frequency aperture  $f(2)f(1)$ , the group delay can, in practice, be obtained approximately by

$$\tau_g = -\frac{1}{2\pi} \left( \frac{\phi_{21}(2) - \phi_{21}(1)}{f(2) - f(1)} \right) \quad (11)$$

### 3.1. Intedigitalinterferometer. design and measurement

The structure shown in figure 3 was etched on only one side of an RT/duroid 6010 with relative permittivity  $\epsilon_r = 10.8$ , dielectric thickness  $h = 0.64$  mm, conductor thickness  $t = 35\mu\text{m}$ ,  $w = 0.3$  mm,  $s = 0.3$  mm and  $L = 99$  mm. In order to find the line impedance and delay the simulation was carried out varying the finger length  $\ell$  from 0.6 to 4.2 mm and keeping all the other parameters fixed. The devices were fabricated, measured and simulated.

The simulation used sonnet software in order to find the magnitude and phase of the  $S$ -parameters, assuming a lossless conductor. Afterwards, equations 10 and 11 were used to find  $Z_0$  and  $\tau_g$ , respectively. In the experimental procedure each device was connected with coaxial connectors to a HP8720A network analyzer. After carrying out a proper calibration, the devices were then measured. This way, the group delay measurement was implemented, and figure 4 summarizes the group delay results from both measurement and simulation for a frequency range of 0.5-3 GHz. As the finger length increases the lumped capacitance per unit length increases. It slows down the group velocity leading to an increase in the group delay. The longer the finger length, compared to the finger width, the closer it is to a purely capacitive element.

The experimental data of  $Z_0$  were obtained using a reflection measurement in time domain low pass function of the HP8720A. The same devices were all measured again and the results are summarized in figure 5. Looking at the beginning of the curve on the left hand side, the figure 5 seems to agree with the classical coplanar strips formulation, as we found  $Z_0 = 99 \Omega$  for  $\ell = 0$  [13]. As we expected,  $Z_0$  decreased as the finger length increased, due to the rise in  $2C_0/d$ , achieving  $50 \Omega$  at  $\ell = 3.9 \text{ mm}$ . As the finger length goes from 0.6 mm to 4.2 mm,  $\tau_g$  increases about 150% and  $Z_0$  decreases about 45%.

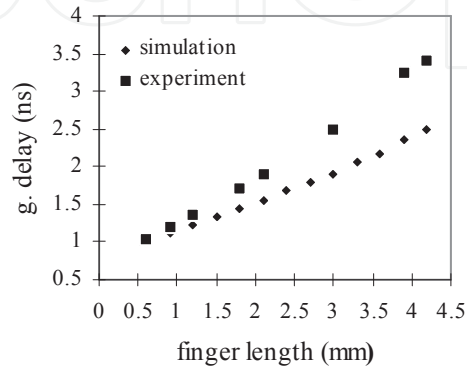


**Figure 4.** Group delay as a function of finger length at a frequency range of 0.5-3 GHz.

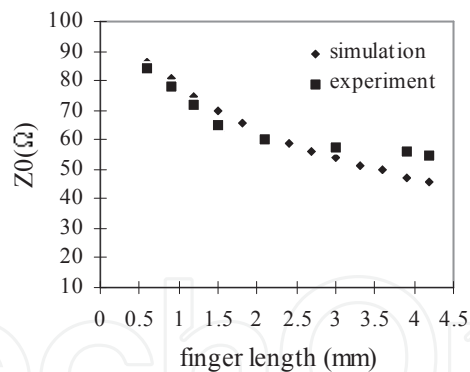


**Figure 5.** Characteristic Impedance as a function of finger length at a frequency range of 0.5-3 GHz.

These results look promising as far as an IFM application is concerned. Referring to a single stage of a typical IFM, a coplanar unequal output impedance power splitter can be designed to feed two delays with different characteristic impedances. The length of the second delay of each discriminator may be increased to achieve better resolution. The results from figures 4 and 5 may be used together to redesign the coplanar unequal output impedance power splitter to achieve the exact impedance matching. Figure 6 shows a prototype system fabricated based on results of figures 4 and 5. Coplanar wave guide, coplanar strips, coplanar unequal output impedance power splitter and coplanar interdigital delay line are integrated

without bends or air bridges. The chip resistors used to increase the isolations between the outputs of the power splitter (and the input of the combiner) are not shown below.

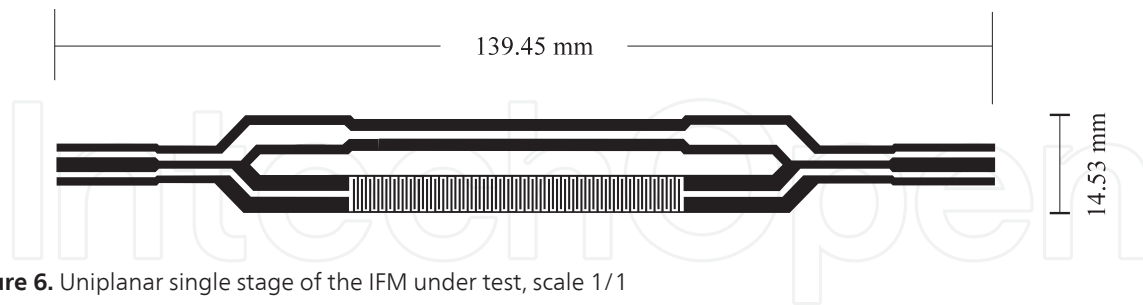


Figure 6. Uniplanar single stage of the IFM under test, scale 1/1

The design has a delay difference of 1.6ns. Two output traces versus frequency from 1.5GHz to 3GHz are presented in figure 7. The theoretical one was obtained using the design equations for a single stage of a typical IFM subsystem [14]. The oscillations in the experimental trace originated from the coaxial connections and the chip resistors bonds.

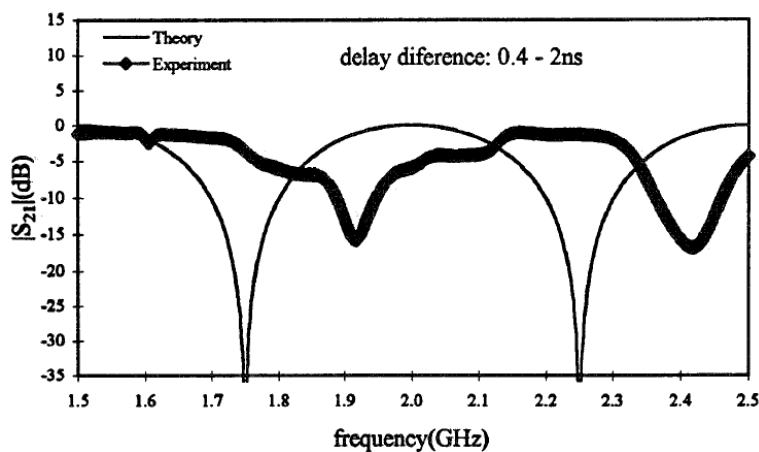


Figure 7. Theoretical interferometer output and measured scattering parameter in dB versus frequency.

#### 4. Interferometer based on band-stop filter for IFM

The IFMS presented now is based on band-stop filter and is shown in Fig. 8. The advantage of using the new architecture is that one has in each channel only multi band-stop filters instead of delay lines and power splitter, as one finds in classical IFMS.

Each word is assigned to only one frequency sub-band to generate a one-step binary code. The response of each multi band-stop filter should be like the one shown in Fig. 9 (a) with discriminators 0, 1, 2, 3 and 4. The discriminator 0 provides the least-significant bit (LSB) and the discriminator 4 provides the most-significant bit (MSB). The form of these responses is suitable to implement the 1 bit A/D converters. Here, let us attribute value 1 if the inser-

tion loss response for the multi band-stop filter is greater than 5 dB, and value 0 for the opposite case. Fig. 9(b) shows the wave form of each 1 bit A/D converter output. According to this example the waveforms at the 1 bit A/D converter outputs are shown in Fig. 9(c). As seen in Fig. 4, this subsystem has its operating band from 2 to 4 GHz, which was divided into 32 sub-bands. Therefore, the resolution obtained was  $f_R = 62.5$  MHz.

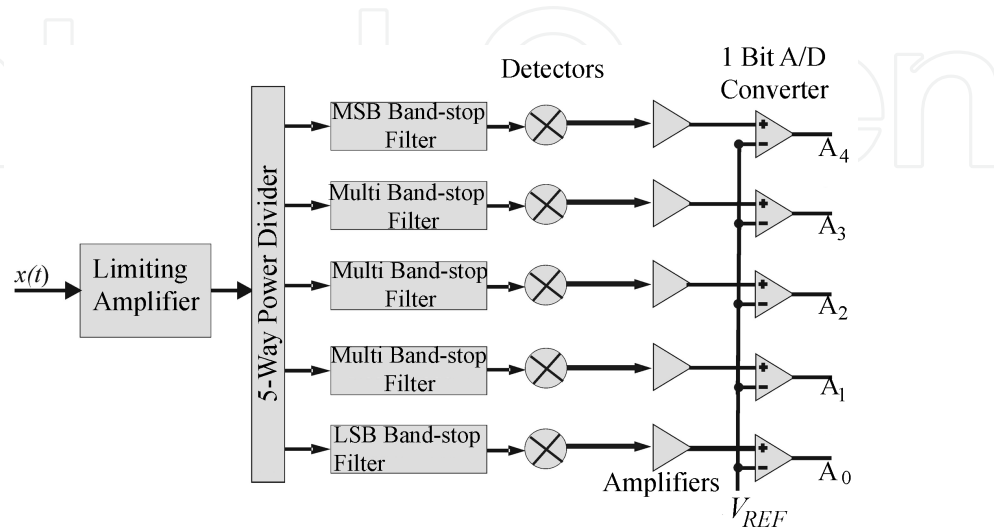


**Figure 8.** Architecture of an instantaneous frequency measurement subsystem (IFMS) using band-stop filters.

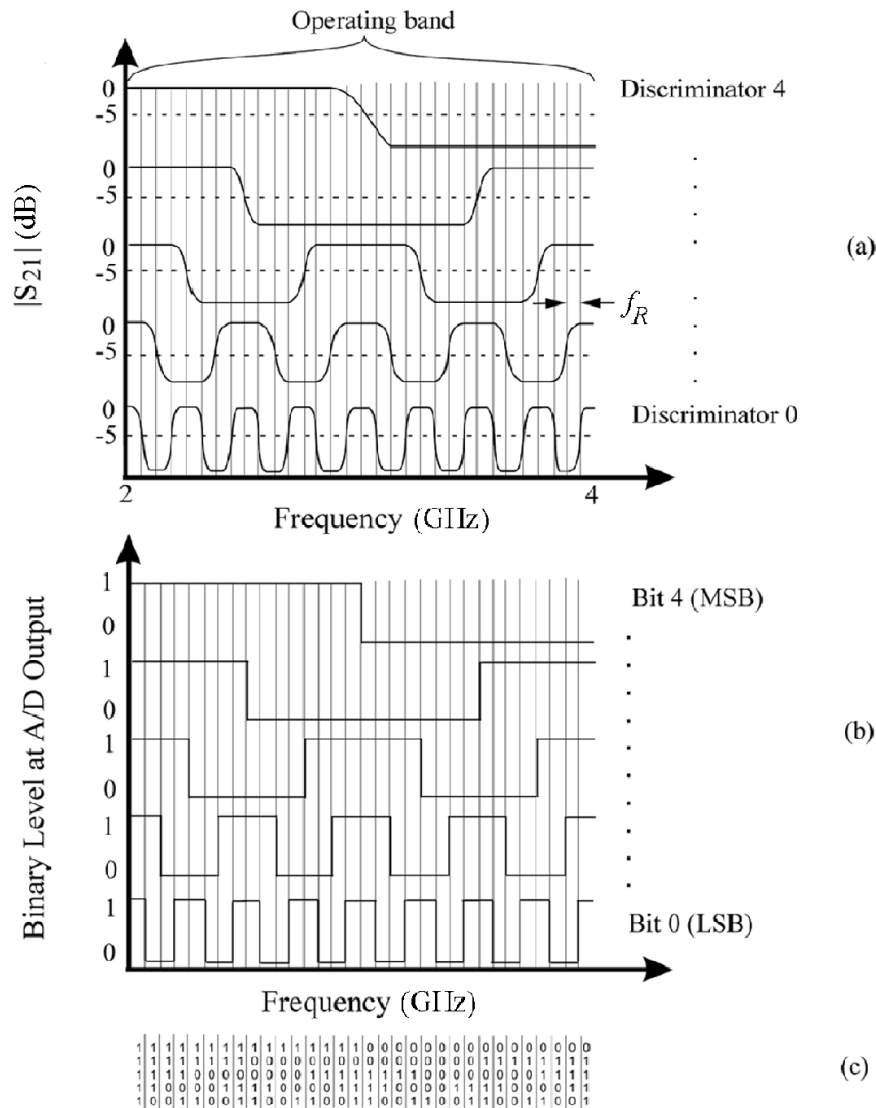
#### 4.1. Multi band-stop filter design and measurement

Rectangular microstrip open loop resonators were chosen to design every discriminator of a five bit IFMS. Frequency response of those resonators presents a narrow rejection band and wide pass band [5] with first spurious out of the working band. Fig. 10(a) shows the top view of a resonator with resonance frequency at 1.9375 GHz. One can see in Fig. 10(b) that the first spurious occurs at 6.140 GHz. Still in this section, it will be shown how this response makes possible the fabrication of a wideband discriminator.

That resonator is placed near to a  $50 \Omega$  microstrip transmission line, which was designed with aid of quasi-static analysis and quasi-TEM approximation [8]-[9]. Fig. 11 shows the resonance frequency adjusted by the length  $l_1 + l_2 + l_3 + l_4$  of the resonator, which must be approximately half wavelength long [8]. Additionally, there is a coupling gap  $g$  given by  $l_2 - l_3 - l_4$ . Moreover, the coupling distance between the resonator and the main transmission line affects this resonance frequency. This distance also affects the bandwidth of the resonator [8].

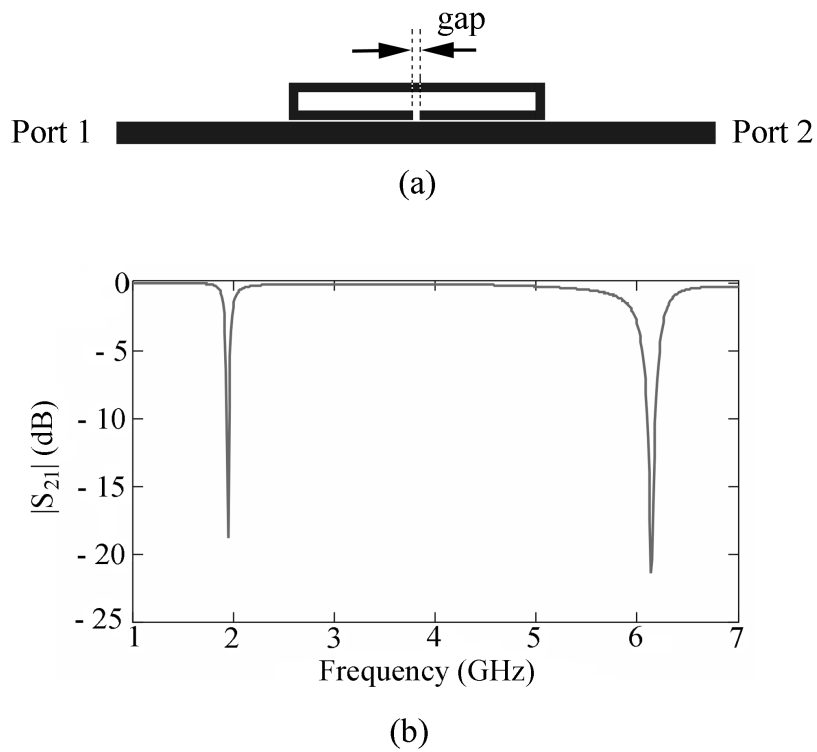
Despite the narrow band of the isolated resonators, wide rejection bands are created from coupled arrays. Fig. 12(a) presents 3 sketches of one, two and three resonators, whose resonant frequencies are 2.02, 2.07 and 2.12 GHz, respectively. The line width for the resonators is fixed to be 0.5 mm along this chapter. The ideal coupling distance between resonators is obtained varying  $d_{ij}$  using EM full wave software.

Fig. 12(b) shows the frequency response obtained at ideal coupling distance between them. These distances are chosen to obtain the insertion loss greater than 10 dB over rejection band and also to get this band as large as required. One notices that the coupling between non-adjacent resonators is almost zero. This happens because their resonance frequencies are not very close and the distance between them is large enough. Therefore, the insertion of a new resonator does not change the position of the others already inserted.



**Figure 9.** Responses for the IFMS from Fig. 8: (a) desired  $|S_{21}|$ , (b) A/D converters output, and (c) generated code.

A model of two coupled resonators has been developed by the authors and will be presented in the full chapter.



**Figure 10.** (a) Physical structure of a resonator with resonance frequency at 1.9375 GHz, and (b) frequency response of the resonator over a wideband.

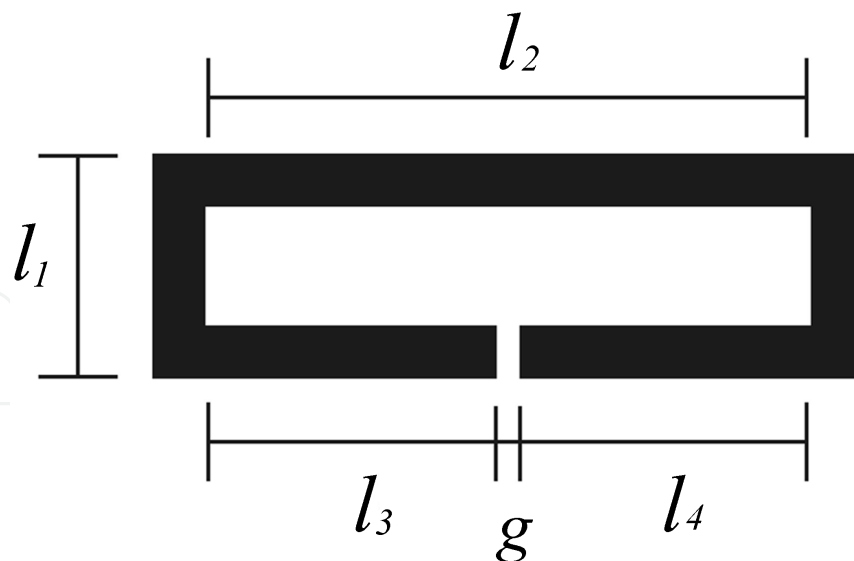


**Figure 11.** Open loop resonator.

As the desired insertion loss of the discriminator is shown in Fig. 9(a), there must be four rejection bands, where the first one is from 2.125 GHz to 2.375 GHz, regarding the chosen operating band. The resonators are arranged one by one. Fig.13 (a) shows this discriminator

with its numbered resonators. The device is designed on a RT6010.2 substrate of relative dielectric constant  $\epsilon_r = 10.2$  and thickness  $h = 1.27$  mm. The  $50 \Omega$  transmission line width is 1.2 mm. The gap of every resonator and the distance between the main transmission line and the resonators are kept 0.1 mm for whole structure. Table I shows the coupling distances between the resonators for this device.

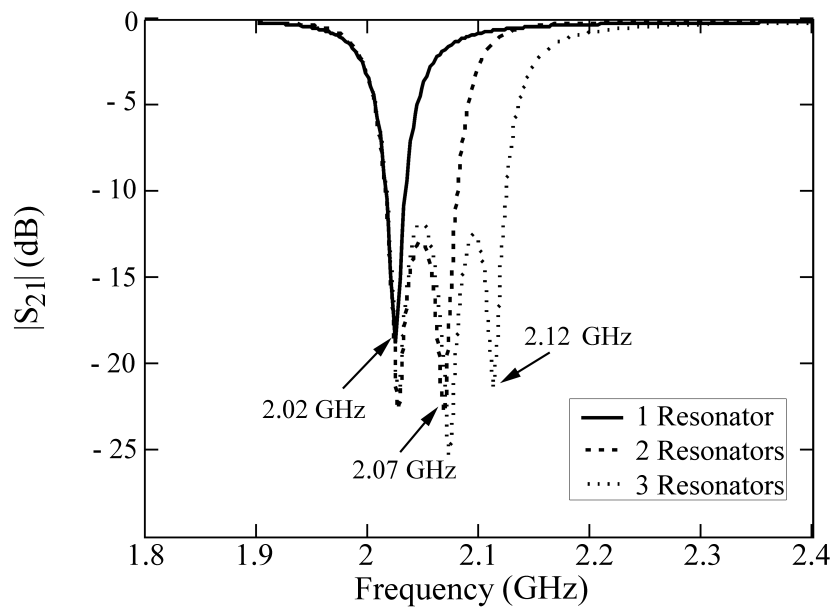
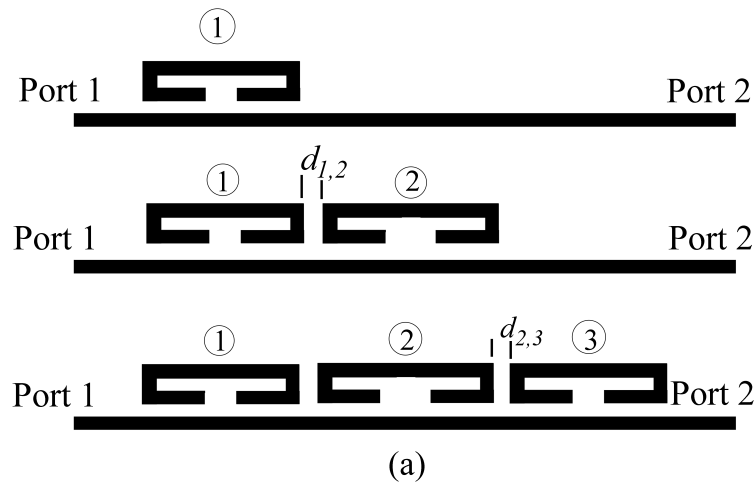


**Figure 12.** (a) The open loop resonator arrays. The scale has been enhanced for a better comprehension of the devices, and (b) frequency response of 1, 2, and 3 resonators.

Still in Fig. 13(a) one sees four groups of resonators, whose frequency responses and A/D converter outputs are shown in Fig. 15(b). Looking carefully their correlation, Group 1 gives

the rejection band over 2 GHz; Group 2 gives the rejection band over 2.5 GHz, and so on. Fig. 13(b) presents the simulated results of the discriminator 1, which agree with the results shown in Fig. 9. One can see the insertion loss level is greater than 10 dB over all rejection bands, and is less than 5 dB over the pass bands. The output A/D converter should generate level zero for  $|S_{21}| < -5$  dB and level 1 for  $|S_{21}| > -5$  dB. Concerning all the involved  $d_{i,j}$ , the dimensions of this discriminator are 3 cm wide and 15 cm long. Following the same procedure, the others discriminators are projected, where new resonators configurations will give new desired rejection bands.

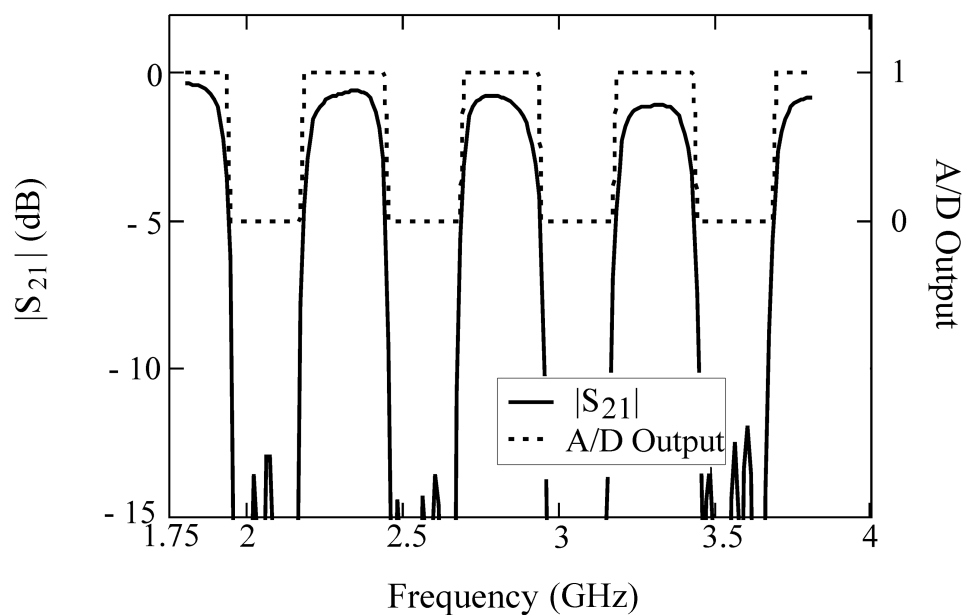
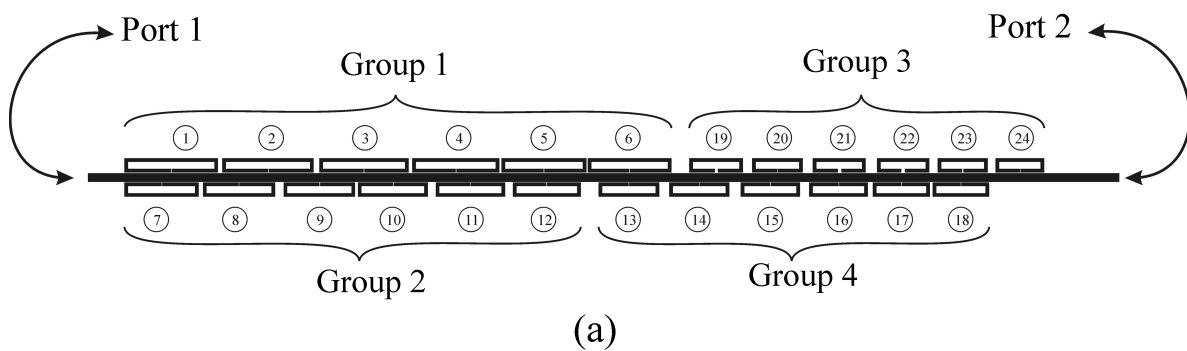


**Figure 13.** (a) Layout of the discriminator 1, and (b) frequency response of the discriminator 1, and the output of the 1-bit A/D converter; 250 MHz for each rejected band.

Coupling distance between "i" and "j" resonators (mm)	
$d_{1,2} = 0.6$	$d_{13,14} = 1.4$
$d_{2,3} = 0.8$	$d_{14,15} = 1.6$
$d_{3,4} = 0.5$	$d_{15,16} = 1.3$
$d_{4,5} = 0.3$	$d_{16,17} = 0.7$
$d_{5,6} = 0.2$	$d_{17,18} = 0.4$
$d_{7,8} = 0.6$	$d_{19,20} = 1.3$
$d_{8,9} = 1.2$	$d_{20,21} = 1.4$
$d_{9,10} = 0.4$	$d_{21,22} = 1.6$
$d_{10,11} = 1.1$	$d_{22,23} = 1.2$
$d_{11,12} = 1.1$	$d_{23,24} = 1.1$

**Table 1.** Coupling Distances

The Fig. 14(a)-(e) presents all the projected IFMS discriminators from Fig. 8, having between 23 and 25 resonators. The number of resonators depends on the desired rejection bands. Following the same principle, each group gives only one rejection band, so that discriminators with eight groups have eight rejection bands, as shown in Fig. 14(e). The others, without any specified group, have only one as shown in Fig. 14 (a) and (b). Fig. 15 shows that the simulated and measured results of the five discriminators are in reasonable agreement with each other.

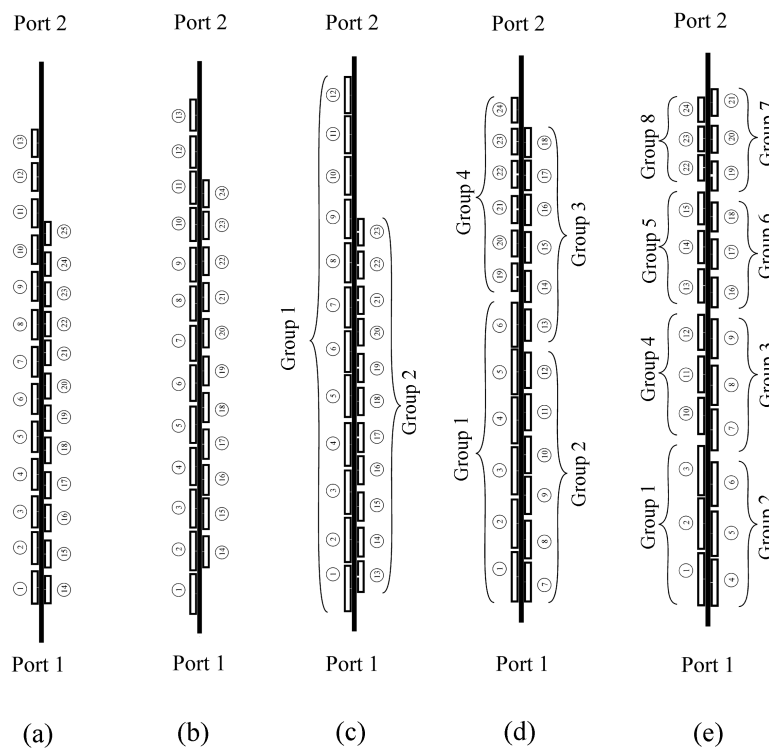


**Figure 14.** Bandstop filters for implementation of the: (a) discriminator 4 – MSB, (b) discriminator 3, (c) discriminator 2, (d) discriminator 1, and (e) discriminator 0 – LSB.

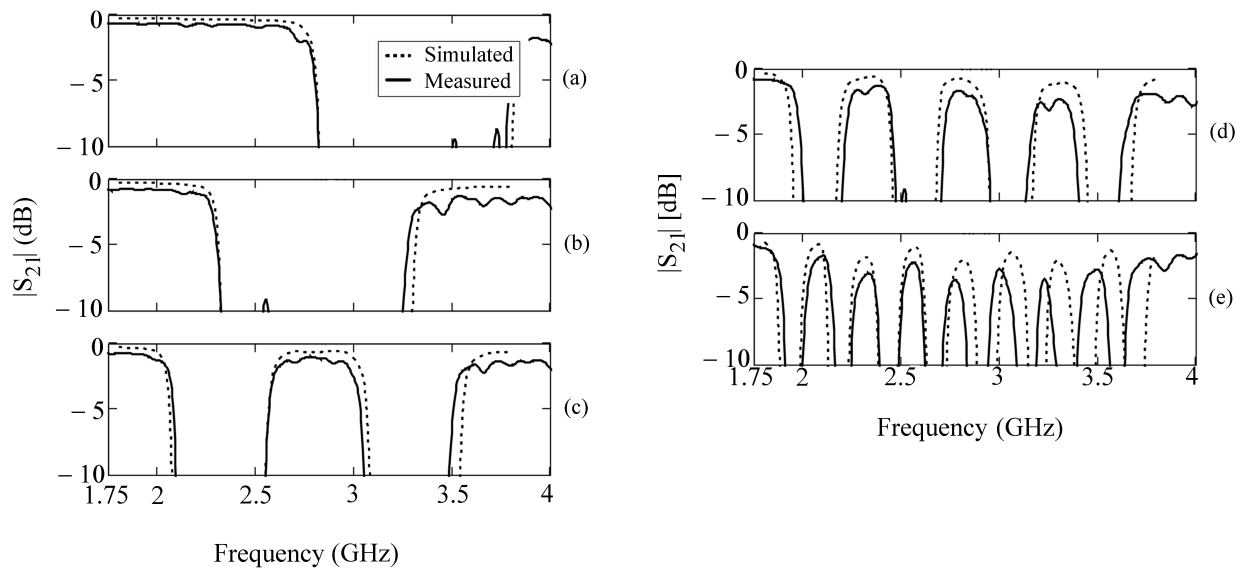


**Figure 15.** Frequency response of the: (A) Discriminator 4 – MSB, (B) Discriminator 3, (C) Discriminator 2, (D) Discriminator 1, and (E) Discriminator 0 – LSB.

## 5. Reconfigurable Frequency Measurement (RFM) designs

Fixed IFM designs like the ones discussed in section IV have the advantage of providing instantaneous frequency identification while reconfigurable designs should do a sweep but are very compact in size, making them suitable for portable and handheld systems. RFMs include tuning elements [15] embedded in the designs to produce multibit frequency identification using reconfigurable measurement branches.

An example of RFM architecture is shown in Fig. 16, this design includes a reconfigurable phase shifter used to produce more than one bit. The number of bits will depend on the amount of phase shifts produced by the reconfigurable design; each phase shift will correspond to a specific control voltage in the case of varactors, otherwise switches will be in “on” or “off” state to produce the different phase shifts. The other components shown in Fig. 16 operate in a similar way to the ones exposed in section IV. The RFM can also include reconfigurable bandstop filters [16] instead of the phase shifter to produce a branch that can produce more than one bit as an alternative design.

The switching speed of the tuning elements used in the reconfigurable phase shifter design will mainly determine the detection speed of the subsystem. Solid state components like PIN, varactor diodes, transistors and the use of ferroelectric materials will provide high tuning speeds, ( $10^{-6}$  seconds for the PIN and varactor diodes,  $10^{-9}$  seconds for transistors and  $10^{-10}$  seconds for the ferroelectric varactors) while the Micro Electromechanical Systems (MEMS) counterpart will provide slower tuning speeds ( $10^{-5}$  seconds) but with the advantage of low power consumption compared with the solid state components. The use of ferroelectric materials results in high tuning speeds with the drawback of having generally high

dielectric losses. When designing an RFM it is important to decide which type of technology is adequate for a given application in terms of detection speed, power consumption and device size.

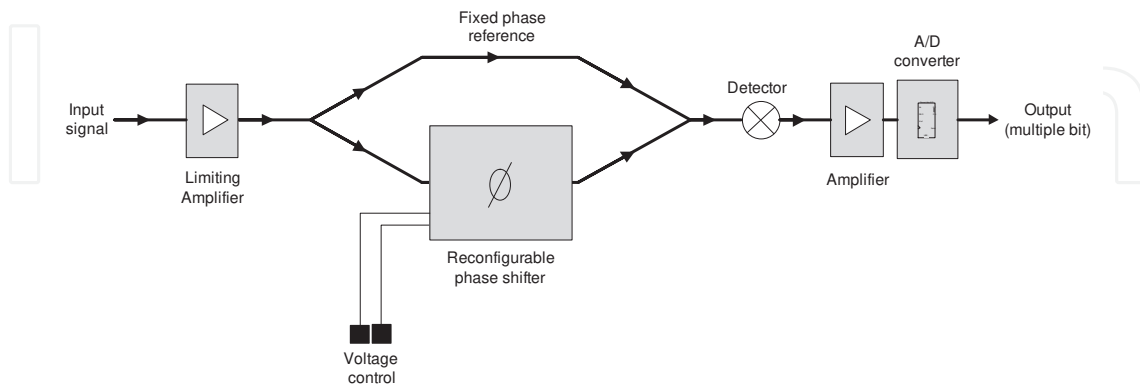


**Figure 16.** Architecture of a reconfigurable frequency measurement subsystem (RFM) based on phase shifters.

Device size will be mainly determined by the type of technology used to implement the subsystem; the most compact designs can be achieved monolithically, by having the components integrated into a single chip. A monolithic design can include all solid state, MEMS and ferroelectric implementations. Hybrid integrations use microwave laminates or substrates and tuning elements, these include solid state, MEMS and ferroelectric surface mountable components that can be embedded into the design. Hybrid integrations normally involve much larger circuit size compared to the monolithic counterpart, however these components normally involve low cost and simple manufacturing and prototyping techniques.

The most reliable technology is the solid state transistor and the ferroelectric films, followed by the PIN and varactor diode ending with the MEMS components. MEMS packaging can improve device reliability by avoiding contamination or humidity of the movable parts of a switch or varactor. The objective of an RFM is to reduce the size of fixed IFMs by designing branches that can produce more than one bit in the identification subsystem. Size reduction is the main advantage of an RFM over a fixed IFM. A disadvantage over fixed IFMs is that there will be a switching time for the device, so the frequency measurement is not instantaneous.

## 6. Final considerations

This chapter presented two kinds of interferometers for IFM applications, the first type was a Coplanar Intedigital Interferometer and the second one was based on Multi band-stop filters, which can substitute the interferometers in the IFM Architecture. For the first case, coplanar strips interdigital delay lines were fabricated, simulated and measured at a frequency

range of 0.5-3 GHz. As the finger length varied from 0.6 mm to 4.2 mm, keeping all the other parameters fixed, the group delay increased by about 150% and the characteristic impedance decreased about 45%. A prototype of uniplanar IFM with a delay difference of 1.6ns was fabricated and measured based on the results of the characteristic impedance and the group delay.

For the second case, Multi band-stop filters were designed, simulated and measured over a frequency range of 2 GHz. The results show that the use of loop resonators to design the discriminators, instead of delay lines and power splitters, make the simulation and the fabrication easier, as there are no more bends or sloping strips. In addition, one has more control over the resolution, as one can couple the resonators one by one and create the rejection bands. In this process, the association of loop resonators was used to design multi band-stop filters. In light of the above, the use of multi band-stop looks promising as far as planar interferometer identifier is concerned.

The use of loop resonators instead of delay lines and power dividers/combiners, to design IFM systems, decreases the simulating time of the whole structure, as there are no more bends or sloping strips. In addition, one has more control over the resolution, as one can couple the resonators one by one and create the rejection bands. The multi-band-stop filters can substitute interferometers in the IFM system architecture, in a very efficient way. Reconfigurable frequency measurement circuits can considerably reduce the size of the IFMs by using tuning elements embedded into the topologies, resulting in multiple bit circuits by means of reconfigurable frequency measurement branches. RFMs switch between states, thus tuning speed determines the sweep time required for signal detection.

## Author details

M. T. de Melo<sup>1\*</sup>, B. G. M. de Oliveira<sup>1</sup>, Ignacio Llamas-Garro<sup>2</sup> and Moises Espinosa-Espinosa<sup>2</sup>

\*Address all correspondence to: marcostdemelo@gmail.com

<sup>1</sup> Federal University of Pernambuco, PE, Recife, Brazil

<sup>2</sup> Centre Tecnològic de Telecomunicacions de Catalunya (CTTC), Communications Subsystems, Castelldefels, Spain

## References

- [1] Tsui J. B. Y. Microwave receivers with electronic warfare applications. New York, NY: John Wiley & Sons, 1986.
- [2] Weiss A. J. and Friedlander B. Simultaneous Signals in IFM receivers. IEE Proc. Radar, Sonar Navig. 1997, vol. 144, no. 4, August.

- [3] Pandolfi C., Fitini, E., Gabrielli G., Megna E. and Zaccaron A. Comparison of Analog IFM and Digital Frequency Measurement Receivers for Electronic Warfare. Proc. 7th European Radar Conference 2010, pp. 232-235, October 2010.
- [4] Biehl M., Vogt A., Herwig R., Neuhaus M., Crocoll E., Lochschmied R., Scherer T. and Jutzi W. A 4 Bit Instantaneous Frequency Meter at 10 GHz with Coplanar YBCO Delay Lines. IEEE Trans. on Applied Superconductivity 1995, June, vol. 5, no. 2, pp. 2279-2282.
- [5] Biehl M., Crocoll E., Neuhaus M., Scherer T. and Jutzi W. A Superconducting 4 Bit Instantaneous Frequency Meter at 10 GHz with Integrated Resistors and Air-Bridges. Applied Superconductivity 1999, October, vol. 6, nos. 10-12, pp. 547-551.
- [6] Wang Y., Su H. T., Huang F. and Lancaster M. J. Wide-Band Superconducting Coplanar Delay Lines, IEEE Trans. on Microwave Theory and Techniques 2005, July, vol. 53, no. 7, pp. 2348-2354.
- [7] de Melo M. T., Lancaster M. J. and Hong J. S., Coplanar Strips Interdigital Delay Line for Instantaneous Frequency Measurement Systems, The Institution of Electrical Engineers, London, Digest, reference number: 1996/226, pp. 1/1-1/4, November, 1996.
- [8] De Oliveira B. G. M., Silva F. B., de Melo M. T. and Novo L. R. G. S. L. A New Coplanar Interferometer for a 5–6 GHz Instantaneous Frequency Measurement System. Proc. 2009 SBMO/IEEE MTT-S International Microwave and Optoelectronics Conference, pp. 591-594, November 2009.
- [9] de Souza M. F. A., e Silva F. R. L. and de Melo M. T. A Novel LSB Discriminator for a 5-bit IFM Subsystem Based on Microstrip Band-Stop Filter. Proc. 2008 European Microwave Week, pp. 36-39, October 2008.
- [10] de Souza M. F. A., e Silva F. R. L., de Melo M. T. and Novo L. R. G. S. L. Discriminators for Instantaneous Frequency Measurement Subsystem Based on Open Loop Resonators. IEEE Transactions on Microwave and Theory and Techniques 2009, September, vol. 57, no. 9, pp. 2224-2231.
- [11] Collin R. E. Foundation for Microwave Engineering. McGraw-Hill; 1992.
- [12] Kiziloglu K., Dagli N., Matthaei G. L. and Long S. I. Experimental analysis of transmission line parameters in high-speed gas digital circuit interconnects 1991. IEEE Trans., MTT-39, pp. 1361-1367.
- [13] Wen C. P. Coplanar waveguide: a surface strip transmission line suitable for nonreciprocal gyromagnetic device applications 1969. IEEE Trans., MTT-17, pp. 1087-1090.
- [14] East P. W. Design techniques and performance of digital IFM, IEE Proc., Vol. 129, Pt. F, No. 3, June, 1982.
- [15] Minin I., editor. Microwave and Millimeter Wave Technologies: from Photonic Bandgap Devices to Antenna and Applications. Reconfigurable Microwave Filters, Ignacio Llamas-Garro and Zabdiel Brito-Brito In-Tech, March 2010.

- [16] Carles Musoll-Anguiano, Ignacio Llamas-Garro, Zabdiel Brito-Brito, Lluís Pradell, Alonso Corona-Chavez, "Fully Adaptable Bandstop Filter using Varactor Diodes", *Microwave and Optical Technology Letters*, Vol. 52, No. 3, March 2010, pp. 554-558.

IntechOpen

IntechOpen